This is a repository copy of *Effect of the ultrastructure of chitosan nanoparticles in colloidal stability, quorum quenching and antibacterial activities*.

White Rose Research Online URL for this paper:
http://eprints.whiterose.ac.uk/150461/

Version: Accepted Version

Effect of the ultrastructure of chitosan nanoparticles in colloidal stability, quorum quenching and antibacterial activities

Vila-Sanjurjo C[1,2]., David L.[2], Remuñán-López C.[3], Vila-Sanjurjo A.[4], Goycoolea F.M.[1,5]*

[1]Westfälische Wilhelms Universität Münster. IBBP. Laboratory of Nanobiotechnology. Schlossplatz 8. Münster, 48143. Germany

[2]Ingénierie des Matériaux Polymères IMP@Lyon1, CNRS UMR 5223, Univ Lyon, Université Claude Bernard Lyon 1,
15, Bd A. Latarjet 69622 Villeurbanne Cedex, France

[3]Department of Pharmacy and Pharmaceutical Technology. Universidade de Santiago de Compostela. Campus Vida, s/n, 15782 Santiago de Compostela, Spain

[4]Grupo GIBE. Departamento de Bioloxía Celular e Molecular, Centro de Investigacións Científicas Avanzadas (CICA). Universidade da Coruña. Campus Zapateira, s/n, 15071 A Coruña, Spain.

[5] School of Food Science and Nutrition. University of Leeds. Leeds LS2 9JT. United Kingdom

*Author for correspondence: F.M.Goycoolea@leeds.ac.uk

ABSTRACT

We have fabricated two types of crosslinked chitosan-based nanoparticles (NPs), namely 1) ionically crosslinked with tripolyphosphate (TPP), designated as IC-NPs and 2) dually co-crosslinked (ionically and covalently with TPP and genipin, respectively) termed CC-NPs. The two types of NPs were physichochemically characterized by means of DLS-NIBS, synchrotron SAXS and M3-PALS (zeta potential). First, we found that covalent co-crosslinking of ionically pre-crosslinked nanoparticles yielded monodisperse CC-NPs in the size range of ~200 nm, whereas the parental IC-NPs remained highly polydisperse. While both types of chitosan nanoparticles displayed a core-shell structure, as determined by synchrotron SAXS, only the structure of CC-NPs remained stable at long incubation times. This enhanced structural robustness of CC-NPs was likely responsible of their superior colloidal stability even in biological medium. Second, we explored the antimicrobial and quorum sensing inhibition activity of both types of nanoparticles. We found that CC-NPs had lower long-term toxicity than IC-NPs. In contrast, sub-lethal doses of IC-NPs consistently displayed higher levels of quorum quenching activity than CC-NPs. Thus, this work underscores the influence of the NP's ultrastructure on their colloidal and biological properties. While the cellular and molecular mechanisms at play are yet to be fully elucidated, our results broaden the spectrum of use of chitosan-based nanobiomaterialsin the development of antibiotic-free approaches against Gram-negative pathogenic bacteria.

ABBREVIATIONS

ζ-potential, zeta potential;

AHL, may refer to acyl-homoserine lactone, N-(3-oxohexanoyl)-L-homoserine lactone, or 3OC6HSL;

a.u., arbitrary units;

CCD, charge-coupled device;

CC-NPs, covalently crosslinked chitosan nanoparticles;

CS, chitosan;

DLS-NIBS, dynamic light scattering with non-invasive light scattering;

ESRF, European Synchrotron Radiation Facility;

FI, fluorescence intensity;

FI/OD_{600}, density-normalized fluorescence intensity;

GNP, genipin;

IC-NPs, ionically crosslinked chitosan nanoparticles; kcps, kilo counts per second;

NPs, nanoparticles;

M3-PALS, mixed-mode phase-analysis light scattering;

PdI, polydispersity index;

OD_{600}, optical density at $\lambda=600$ nm;

OD_{t0}, initial optical density;

QQ, quorum quenching;

QS, quorum sensing;

SAXS, small-angle X-ray scattering;

TEM, transmission electron microscopy;

TPP, sodium tripolyphosphate.

INTRODUCTION

The abuse of antibiotic therapies as a strategy to combat bacterial pathogens for many decades has led to major public health concerns regarding the spreading of bacterial drug resistance. As a result, numerous calls in favor of the urgent pursuit of alternative antimicrobial strategies are now widespread [1, 2]. Among these, strategies directed to interfere with bacterial quorum sensing (QS), also called quorum quenching (QQ), are of particular interest [3, 4]. The term QS comprises several mechanisms of cell-to-cell communication mediated by exocellular chemical compounds that act as autoinducers [5, 6]. Acyl-homoserine lactones (AHLs), initially described in the marine bioluminescent bacterium *Vibrio fischeri* [6], constitute the best-known family of autoinducers. Together with the rest of the QS machinery of *V. fischeri*, composed of the proteins LuxI and LuxR, AHLs are evolutionary well conserved among Gram-negative bacteria [6, 7]. AHLs are synthesized by LuxI-type enzymes and can freely diffuse in and out of the cell, where they bind to LuxR-type activators to regulate communal behavior [6, 7]. As such, AHL-based signaling is a bacterial communication strategy consisting in the integration of the environmental concentration of signal as a surrogate of cell density. QS is involved in many pathogenic processes in bacteria, including the production of virulence factors, biofilm formation, and bacteria-host interactions among others [8, 9]. QQ strategies include the use of agents capable of blocking QS-based mechanisms by inactivating the signaling molecules, interfering with signal reception, or inhibiting signal synthesis [3, 10, 11].

Chitosan (CS) refers to a family of aminopolysaccharides obtained by partial chemical deacetylation of chitin. This biopolymer is composed of linear chains of β-1,4-linked glucosamine and N-acetyl-D-glucosamine units. The properties of chitosan mainly depend on its molecular

weight, polydispersity, and the molar fraction of acetylated units, together with their distribution pattern. Ionic (also known as physical) or chemical crosslinking may be applied in order to improve or modulate the characteristics of CS and to design novel CS-based platforms intended for biopharmaceutical applications [12]. Ionic crosslinking of CS has been widely described for the development of non-toxic, CS-based hydrogels, as well as for the preparation of CS-based micro- and nano-systems [13-19]. The mild conditions involved in ionic crosslinking makes this method optimal for the encapsulation and protection of delicate therapeutic biomolecules (biologics), such as peptides, proteins and nucleic acids [20-23]. Ionic crosslinking of CS is normally performed by using either multivalent anions or polyanions, such as tripolyphosphate (TPP). After finding the optimal physico-chemical and processing parameters, particles in the micro- or nano-meter range can be created by ionic gelation of CS with TPP [13, 15, 24-27] .

The use of chemical crosslinkers is known to improve the stability of CS against pH, temperature variations, and biological and mechanical degradation, while allowing to modulate structure and properties of the CS gel network [14, 28-34]. In fact, by controlling the extent of chemical crosslinking of CS, it is possible to constraint important features of CS-based materials such as size, which may range from nanoparticles to macroscopic gels or films, or the extent of association and release of bioactive payloads of interest [31, 32, 35-43]. Genipin (GNP) is a natural crosslinking agent obtained from the glycosylated geniposide iridoid compound produced by the fruits of *Gardenia jasminoides* and *Genipa americana*. GNP has been reported to be much less cytotoxic and more biocompatible than other well-known chemical crosslinkers used in the context of CS, such as glutaraldehyde [30, 32, 40, 44-46]. Thus, the use of GNP as a CS crosslinker has become a promising alternative for developing fully biocompatible CS-based materials. The chemical crosslinking reaction between GNP and CS takes place in two steps. The first and faster step involves a nucleophilic attack by the amino groups of chitosan on the olefinic carbon of GNP,

followed by the opening of the dihydropyran ring and the attack by the secondary amino group of the newly formed aldehyde. The second step, slower than the first one, consists in the nucleophilic substitution of the ester group of GNP, leading to the formation of a secondary amide linkage with CS and of crosslinked bridges [40, 45, 47].

CS has been shown to interfere with biofilm formation [48] and with both biofilm formation and QS [49] in a variety of Gram positive and negative bacteria. However, no studies on the QQ effect of CS-based nanomaterials were reported until very recently. Our group has recently reported that CS oil-core nanocapsules can bind to bacterial cells, promote cell aggregation, and attenuate the QS response of a model biosensor [50]. Here, we describe the preparation and the physicochemical and structural characterization of two types of CS NPs, namely ionically (IC) and chemically co-crosslinked (CC) NPs. By using a model QS biosensor, we demonstrate that IC-NPs constitute a subset of CS-NPs capable to strongly interfere with QS at sublethal doses.

EXPERIMENTAL SECTION

1. Materials

We used a high-purity grade, commercial sample of the hydrochloride salt form of CS (ProtasanUP CL113; Novamatrix, FMC-Biopolymer, Norway; Mw ~92 kDa; Ip ~2.5, as determined by GPC-MALLS-DRI; DA ~14%, as determined by ^{1}H NMR). GNP was purchased from Challenge Bioproducts (Taiwan). Analytical grade TPP, N-(3-oxo-hexanoyl)-L-homoserine lactone (3OC6HSL, named AHL thereafter), and other chemicals were purchased from Sigma-Aldrich (Germany). Milli-Q water was used throughout this work.

2. Preparation and characterization of nanoparticles

2.1. Modulation of ionic strength:

IC-NPs were prepared according to the general ionotropic gelation protocol described by Calvo et al. [15] with minor modifications. To assess the optimal composition for the fabrication of IC-NPs with average size ≤200 nm and with low polydispersity (PdI~0.1-0.2), different CS:TPP mass ratios were screened in water and 85 mM NaCl. To obtain IC-NPs with varying CS:TPP mass ratios (from 2.67:1 to 9.0:1), stock solutions of CS (2-3 mg/mL) and TPP (1-1.25 mg/mL) were prepared both in water and 85 mM NaCl and aliquots of the two components were mixed in 96-well microplates. To rapidly assess the composition of IC-NPs that would yield NPs with the lowest average NP diameter and polydispersity index (PdI), we followed the classification method described by Calvo *et al* and Dmour & Taha [15, 51]. Larger batches (30 mL) of IC-NPs with desired sizes and PdIs, were prepared by pouring 11.25 mL of TPP solution onto 18.75 mL of CS solution under magnetic stirring (500 rpm). When necessary, IC-NPs were isolated by centrifugation (40 min, 10.000 x g, 25 °C) in 1.5 mL vials containing a glycerol bed and the pellets were resuspended in 100 µL of water.

2.2. Covalent GNP co-crosslinking of NPs:

IC-NPs were covalently co-crosslinked with GNP at different GNP:CS mass ratios (0.06:1 – 1.7:1). Aliquots of a 5 mg/mL GNP solution were added to a freshly prepared, non-isolated IC-NP suspension, to a final concentration of 1 mg/mL in water. The mixture was incubated at 37 ºC under shaking (~1400 rpm) for times ranging from 24 to 244 h.

Physicochemical characterization of IC- and CC-NPs:

The size distribution and ζ-potential of the NPs were determined by dynamic light scattering using non-invasive back scattering (DLS-NIBS, measuring angle 173º) and by phase-analysis light scattering (PALS), respectively. In both cases, we used a Malvern Zetasizer NanoZS ZEN 3600 (Malvern Instruments UK) equipped with a 4 mW, He/Ne laser output operating at λ=633 nm. The

Malvern patented, mixed mode measurement method (M3-PALS) was used for PALS analysis. All measurements were performed at 25.0 ± 0.2 ºC. ζ-potential analysis were performed in 1mM KCl and 85 mM NaCl. The value of ζ-potential was derived using Smolouchowski's equation from the electrophoretic mobility measurements, according with the function:

$$U_E = \frac{2 \quad f(Ka)}{3}$$

Eq. 1

where:

U_E = electrophoretic mobility; ε = dielectric constant; ζ = zeta potential; η = Viscosity of solvent; $f(Ka)$ = Henry's function (= 1.5 Smoluchowski approximation for nanoparticles > 200 nm and $I > 10^{-3}$ M).

The kinetics of the crosslinking reaction were monitored by UV/VIS spectroscopy with a Beckman-Coulter DU® DU 730 - Life Science UV/Vis Spectrophotometer and by Synchrotron SAXS at the BM2 D2AM beamline of the ESRF synchrotron (Grenoble, France). For SAXS an incident energy (E) of 16.000 keV, and a sample to detector distance ~1.88 m were used. The I(q) vs. q patterns were obtained with a Roper Scientific CCD camera after performing dark-image subtraction, pixel-sensitivity normalization, and radial averaging around the image centre (centre of gravity of the incident beam) with the BM2IMG software. Q-pixel calibration was performed with silver behenate.

2.3. Determination of the concentration of IC-NPs and CC-NPs:

Batch NP concentration was determined after centrifugation (40 min, 10.000 x g, 25 °C) of fixed volumes of freshly prepared, non-isolated IC-NPs in the absence of glycerol. This was performed in triplicate with tared vials, by discarding the supernatants and dry-weighing the remaining pellets. The batch IC-NP solution with a known concentration of NPs was serially sub-diluted in triplicated vials (dilution factors: 0, 2, 5, 10, 20, 50, 100, 200, 500 and 1000) and the derived count rate (kilo

counts per second; kcps) was estimated for each condition by DLS-NIBS at 25 ℃ and with an attenuator value of 9. Linear regression calibration of the kcps values against NPs is shown in Figure S1. The resulting calibration equation:

$$Derived\ count\ rate\ (Kcps) = 285946 \times [NPs](mg/mL) - 0.9950 \qquad \text{Eq.2}$$

was used to readily estimate the concentration of IC-NPs and CC-NPs from their DLS-NIBS-measured kcps values during subsequent experimental steps (e.g., isolation, covalent crosslinking, dilution, etc.) [52].

2.4. Stability of IC- and CC-NPs in supplemented M9 minimal medium:

IC-NPs, with a CS:TPP mass ratio of 3.3:1, were prepared in 85 mM NaCl from CS and TPP solutions at concentrations of 2 and 1 mg/mL, respectively. The resulting IC-NPs were isolated as explained above and diluted to a final concentration of 1 mg/mL. Isolated IC-NPs were sub-divided into six vials (1 mL each), three of which would be used as controls in the experiments described below. The other three vials were subjected to crosslinking with 60 µL of GNP (5 mg/mL) and incubated for 24 h at 37 ℃ under shaking (100 rpm), to obtain CC-NPs at a GNP:CS mass ratio of 0.3:1. 60 µL of water were added to the control vials instead of GNP and incubated under the same conditions as above. After incubation, the NPs were centrifuged and isolated as explained above and re-suspended in water to a final concentration of 1 mg/mL. All vials were sub-diluted 1:50 in M9 minimal medium supplemented with 0.5% casamino acids, 1 mM thiamine hydrochloride, and ampicillin (200 µg/mL), in a final volume of 1 mL. Control vials were sub-diluted and incubated in water under the same conditions as above. IC-NPs and CC-NPs were incubated under shaking (100 rpm) for 6 h in M9 minimal medium at 37 ℃. The time-resolved evolution of NP size was monitored by DLS-NIBS at 37 ℃.

3. Microbiological assays

3.1. Assays with the E.coli fluorescent biosensor:

The E. coli strain Top10 was transformed with plasmid pSB1A3-BBa_T9002, carrying the BBa_T9002 genetic device (Registry of Standard Biological Parts: http://parts.igem.org/Part:BBa_T9002), kindly donated by Prof. John C. Anderson (UC Berkeley, USA). The transformed strain is a biosensor that can respond to AHL.

To minimize experimental variability, we strictly adhered to the following bacterial seeding protocol. A flask with 10 mL of Luria Bertani (LB) broth, supplemented with 200 µg/mL ampicillin, was inoculated with a single colony from a freshly streaked plate of strain Top10 pSB1A3-BBa_T9002. After incubation for 18 h at 37 ºC with vigorous shaking, 0.5 mL aliquots of the overnight culture were mixed with 0.5 mL of 30 % glycerol and stored at -80 ˚C until further usage. Before each experiment, a glycerol stock from the single colony-culture was diluted by a factor of 10^{-3} into 20 mL of M9 minimal medium supplemented with 0.5% casamino acids, 1 mM thiamine hydrochloride and ampicillin (200 µg/mL) and grown to an OD_{600} of $0.04 \pm 7.76 \times 10^{-3}$ (~4 h). AHL was dissolved in acetonitrile to a stock concentration of 1×10^{-1} M and stored at -20˚C until further usage. Before each experiment, the AHL stock was serially diluted in water to yield a working solution of 1×10^{-8} M. 10 µL of the AHL working solutions and 10 µL of NPs or water (controls), were transferred to the wells of a flat-bottomed 96-well plate (Greiner Bio-One, cat. # M3061). After the addition of a 180 µL aliquot of the bacterial culture to each well, the final AHL concentration became 5×10^{-10} M. Three blank wells with 200 µL of medium were used to measure the absorbance background. Additionally, three control wells containing the biosensor in the absence of AHL were prepared to measure the fluorescence background. The plate was incubated in a Safire Tecan-F129013 Microplate Reader (Tecan, Crailsheim, Germany) at 37 ºC and with vigorous orbital shaking during five seconds prior to each measurement. Absorbance and

fluorescence were measured every six minutes with the following parameters: (fluorescence excitation wavelength λ_{ex} = 485 nm, fluorescence measurement wavelength λ_{em} = 520 nm, integration time = 40 µs, number of flashes = 10, gain = 100, measurement mode = top). To avoid complications due to excessive evaporation during the determinations, only 294 min of growth were recorded and the extent of evaporation was recorded by weighing the microplate before and after incubation (measured evaporation = 6.7 ± 0.27 %; n = 3). For each experiment, fluorescence intensity (FI) and OD_{600} were corrected by subtracting the background values and expressed as the average of a minimum of three biological replicates.

3.2. Determination of antimicrobial activity of CS NPs:

Isolated IC-NPs and CC-NPs were serially diluted in water by a factor of 0, 2, 5, 10 and 20. Following the protocol described in the previous section, ten-µL aliquots of the NP dilutions were applied to triplicated wells containing 180 µL of the E. coli biosensor culture and 10 µL of 1×10^{-8} M AHL (final AHL concentration = 5×10^{-10} M), resulting in a final volume of 200 µL. Control wells in the absence of NPs were prepared by adding 10 µL of water to the culture instead of AHL. Blank and AHL-less control wells were prepared as explained above. Final NP concentrations in the microplate ranged from 6.26 µg/mL to 25.81µg/mL for IC-NPs and from 6.85 to 70.93 µg/mL for CC-NPs. Microplates were incubated in the microplate reader for 300 min, as explained above. To monitor cell viability, 20 µL-aliquots from each treatment were applied to a new microplate containing 180 µL of fresh M9 minimal medium and incubated for further 300 min in the microplate reader. To estimate the effect of the NP treatments on cell growth, the OD_{600} values were plotted against time and the growth curve cell was fitted to the SGompertz function (OriginLab, Northampton, MA):

$$OD_{600} = a \cdot e^{-e\left(k(t-t_c)\right)} \qquad \text{Eq. 3}$$

where:

a = amplitude, or maximum value,

k = growth rate coefficient

t_c = time at inflection

Growth rate values (μ_m) were calculated from the fitted parameters as explained by Tjørve and Tjørve [53]:

$$\mu_m = a\frac{k}{e} \qquad \text{Eq. 4}$$

Statistical comparisons between NP treatments and controls were made with GraphPad Prism version 6.00 (GraphPad Software, La Jolla California USA) using one-way ANOVA together with multiple-comparison Dunnett's Test (** $p \leq 0.01$; *** $p \leq 0.001$; **** $p \leq 0.0001$).

The IC_{50} values for IC-NPs and CC-NPs were calculated as follows. The ratio of the OD_{600} values obtained after a 300-min incubation in fresh medium of NP-pre-treated and control cells were converted to % viability values, plotted against the $\log_{10}$ of NP concentration, and fitted to the non-linear dose-response function ($Y = 100/(1+10^{((LogIC50-X) \times HillSlope)})$), GraphPad version 6.00, GraphPad Software, La Jolla California USA).

3.3. Evaluation of the ability of CS NPs to inhibit the QS response in the E. coli biosensor:

The QS inhibitory activity of IC-NPs and CC-NPs was evaluated as follows. IC-NPs and CC-NPs, prepared and isolated as explained above, were serially diluted in water and 10-μL aliquots of all the dilutions were applied to a microplate containing the E. coli biosensor culture in the presence of 5×10^{-10} M AHL. The plates were incubated for 300 min in the microplate reader as explained above.

RESULTS

Modulation of ionic strength for the optimization of size and polydispersity of ionically, TPP-crosslinked CS NPs (IC-NPs):

The type of high-purity grade hydrochloride salt form of CS (see Experimental Section) has been manufactured to allow its easy dissolution in water [54]. It is known that the ionic strength of the solvent affects the intrinsic viscosity and chain conformation of CS in polyelectrolyte solutions [55]. Huang and Lapitsky [56] have shown that moderate amounts of NaCl enhance the colloidal stability of TPP crosslinked chitosan NPs during their formation, likely by inhibiting the bridging of the newly formed microgels by TPP. In addition, Jonassen et al. [13] have reported that smaller and more compact particles were formed in saline solvents, compared to particles formed in pure water. Building into these studies, and in order to more amply screen the TPP-crosslinking conditions, we explored two parallel fabrication routes, one performed in plain water and the other in 85 mM NaCl, a salt concentration previously used in our lab [57, 58]. In previous studies, we determined that the final pH attained by similar NP formulations prepared with TPP in 85 mM NaCl (CS:TPP mass ratio 6:1) was 5.89 ± 0.06 [58]. While this pH is not far off the pK_o of chitosan in HCl ($\sim 6.0 \pm 0.1$), it has been shown that the nanoparticles remain colloidally stable [58, 59].

When IC-NPs were prepared in water, a clear solution was observed when CS concentrations ranged from 1.5-2.25 mg/mL at a TPP concentration of ≤ 0.3 mg/mL. Aggregation was evident when the concentrations of CS and TPP were between 1.5-2 mg/mL and 0.4-0.5 mg/mL, respectively (see Table S1 and Figure S2A). In the case of the systems prepared in NaCl, clear solutions were observed at CS concentrations below 2.25 mg/mL and TPP concentrations below 0.3 mg/mL. No aggregation occurred at any of the concentrations tested (see Table S1 and Figure S2B). Following Dmour & Taha [51], we searched for relative concentrations of CS and TPP yielding the typical opalescence of colloidal particles in suspension (Tyndall effect). The

concentration ranges at which the Tyndall effect was obvious both in water and 85 mM NaCl is shown in Table S1 and Figure S2.

Next, we confirmed the presence of NPs within these concentration ranges by DLS-NIBS with the Zetasizer NanoZS. According to the manufacturer, the size detection limit of the instrument ranges from 0.3 nm to 10 µm, thus providing a broad detection range for these experiments. The contour plots of Figure 1 illustrate the dependence of the NP size (panels A and B) and polydispersity (panels C and D) on the composition of IC-NPs prepared in water (panels A and C) and in 85 mM NaCl (panels B and D). The plot can be considered as a landscape with hills and valleys representing NP sizes (panels A and B) or PdI values (panels C and D). In this view, the green-to-red colour range represents hills with high NP sizes (panels A and B) or PdI values (panels C and D), whereas the purple-to-blue colour range corresponds to valleys with sub-micron sizes (panels A and B) and low-to-medium PdI values (panels C and D). Comparison of the contour plots obtained in in water and in 85 mM NaCl revealed that the presence of salt played an important role in determining the final size and polydispersity of IC-NPs. Specifically, it was possible to obtain NPs with a size of ~200 nm and a fairly low PdI, ~0.2-0.3, under a narrow range of CS:TPP mass ratios, namely 3:1-4:1 in 85 mM NaCl (dashed lines in panels B and D of Figure 1). In water and under an identical range of composition, NP sizes and PdI values were much larger (dashed lines in panels A and C of Figure 1). These findings are in general accordance with previous studies [13, 54, 56], reporting that the addition of adequate amounts of monovalent ions to NP solutions aids in the optimization of the NP hydrodynamic radius and screens the electrostatic repulsion of the charged amino groups present at the pH of the batch CS solution (pH ~5.0), leading to increased flexibility, larger degree of compaction of the CS backbone, superior colloidal stability, and lower polydispersity [13, 54, 56].

Figure 1E and F summarize the dependence of the average NP diameter on the CS:TPP mass ratios in water and in 85 mM NaCl, respectively. Among the CS:TPP mass ratios lying within the area of the contour plot representing optimal NP size and PdI values in 85 mM NaCl (area within dotted lines in panel F), we chose the 3.33:1 mass ratio for further analysis. The size of the NPs chosen for the fabrication of CC-NPs was 251 ± 99 nm, as determined by DLS-NIBS. None of the IC-NP batches fabricated in plain water were used to make CC-NPs.

Covalent co-crosslinking of IC-NPs produces a defined core-shell structure:

To elucidate whether TPP-crosslinked CS NPs could be co-crosslinked with GNP, salt-prepared IC-NPs with a CS:TPP mass ratio of 3.33:1 (Figure 1F) were covalently co-crosslinked with GNP (GNP:CS mass ratios 0.06:1-1.70:10.3) at 37 °C. UV-VIS spectroscopy performed during the incubation provided clear evidence that CC-NPs were indeed co-crosslinked with GNP (Figure S3).

To gain further insight into the structural modifications that take place within CC-NPs during co-crosslinking with GNP, synchrotron SAXS studies were conducted to probe the ultrastructure of our NPs in the 1-50 nm resolution range. This range would allow us to ascertain, for example, whether there might exist differentially structured regions in our NPs, as opposed to having structurally homogeneous particles. In Figure 2A-C we plotted the scattering patterns $I(q)$ against the scattering vector q (in log-log scales) for CC-NPs at various GNP:CS mass ratios and at different incubation times. Given that significant structural modification of nanogel systems at the molecular scale occurs during stepwise increases of temperature [60], the time-zero plots were deliberately omitted, because the samples were set at room temperature at this time point. The patterns were also characterized with Kratky plots ($I(q) \cdot q^2$ vs. q) [61] (Figure 2D-F). The scattering patterns showed a bell-shaped curve typical of compact nanoparticles, with a prominent peak centred at $q^* \sim 0.01$ Å^{-1} in all cases. The $q^* \sim 0.01$ Å^{-1} peak is absent in the case of uncrosslinked CS solutions, although these solutions exhibit an alternative, weak correlation peak due to
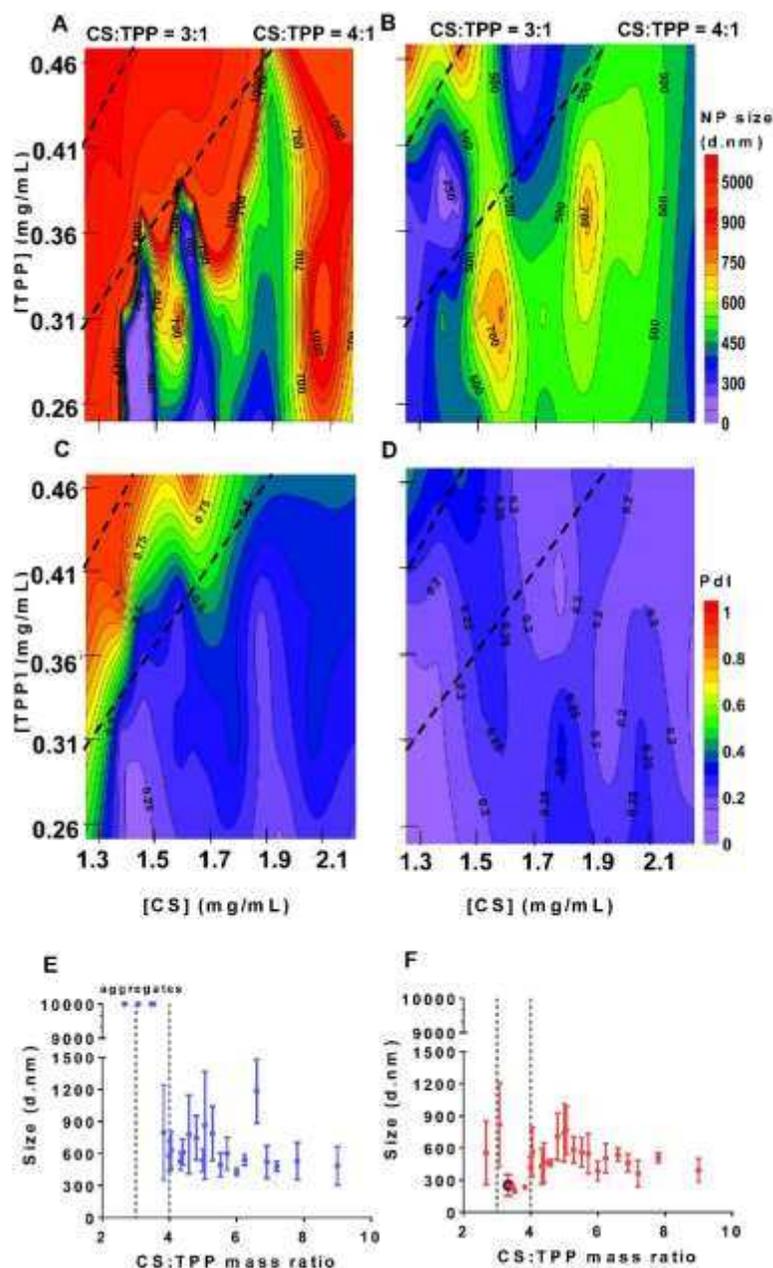
Figure 1. Dependence of IC-NP size (diameter) and PdI on the CS:TPP mass ratio, as determined by DLS-NIBS. A-D. Contour plots showing the dependence of the size (A, B) and PdI (C, D) of IC-NPs on the concentration of CS and TPP in water (A, C) and in 85 mM NaCl (B, D), respectively. X-axes CS concentration in mg/mL (for the sake of clarity only shown in panels C and D). Y-axes TPP concentration in mg/mL (for the sake of clarity only shown in panels A and C). Dashed lines in A-D delimit the area contained within the CS:TPP mass ratio range of 3:1 to 4:1. The identity of the line is indicated on top of the panels A and B. E-F. Variation of NP size in water (E) and in 85 mM NaCl (F) as a function of the CS:TPP mass ratio. X-axis, CS:TPP mass ratio obtained by dividing the relative CS and TPP concentrations in all the systems tested. Y axis, NP size (diameter) in nm. Dotted lines in E and F indicate the CS:TPP mass ratio ranges of 3:1 and 4:1. Data represent the mean and standard deviation of three replicates. The CS:TPP mass ratio of 3.33:1 in 85 mM NaCl is highlighted in black in F.

polyelectrolyte ordering [62]. The value of $q*$ is related to the radius of gyration (Rg) as follows.

For a monodisperse collection of particles, Rg is given by $Rg = \dfrac{\sqrt{3}}{q*}$ [61][9]. Therefore, in our hands,

Rg ~17 nm (Figure 2D-F).

Interestingly, the intensity of the peak is reduced in Kratky plots as GNP:CS mass ratios increased (panels D-F in Figure 2), except for the lowest GNP:CS mass ratio, 0.06. The trend shown in Kratky plots was robust, as it was obtained at the three different incubation times shown in Figure 2D-F. This also indicated that NPs were stable and did not sediment throughout the experiment. The reduced peak intensity observed in Kratky plots at GNP:CS mass ratios higher than 0.06 might stem from a change of the electron-density contrast factor due to increased levels of chemical crosslinking with GNP. Indeed, such crosslinking process could compete with CS/TPP physical interactions and induce TPP release which, in turn, would decrease the mean electron density within the particles.

   To further examine the effect of GNP on the physical structure of the surface-solvent boundary of CC-NPs, we analysed the scattering patterns with a modified Porod law accounting for a core-shell or diffuse interface structure [63].

$$I(q).q^2 = -B + \frac{C}{q^2}$$
Eq. 5

This model allowed us to evaluate the thickness of the interface of the transition layer (i.e., the shell thickness, L_i) using Equation 6:

$$L_i = \sqrt{\frac{12\pi B}{C}}$$
Eq. 6

where C and $-B$ are respectively the slope and intercept of the best linear fit parameters obtained with the modified Porod equation (Equation 5) [64]. Figure 3A-C shows the $I(q)*q^2$ vs. $1/q^2$ plots
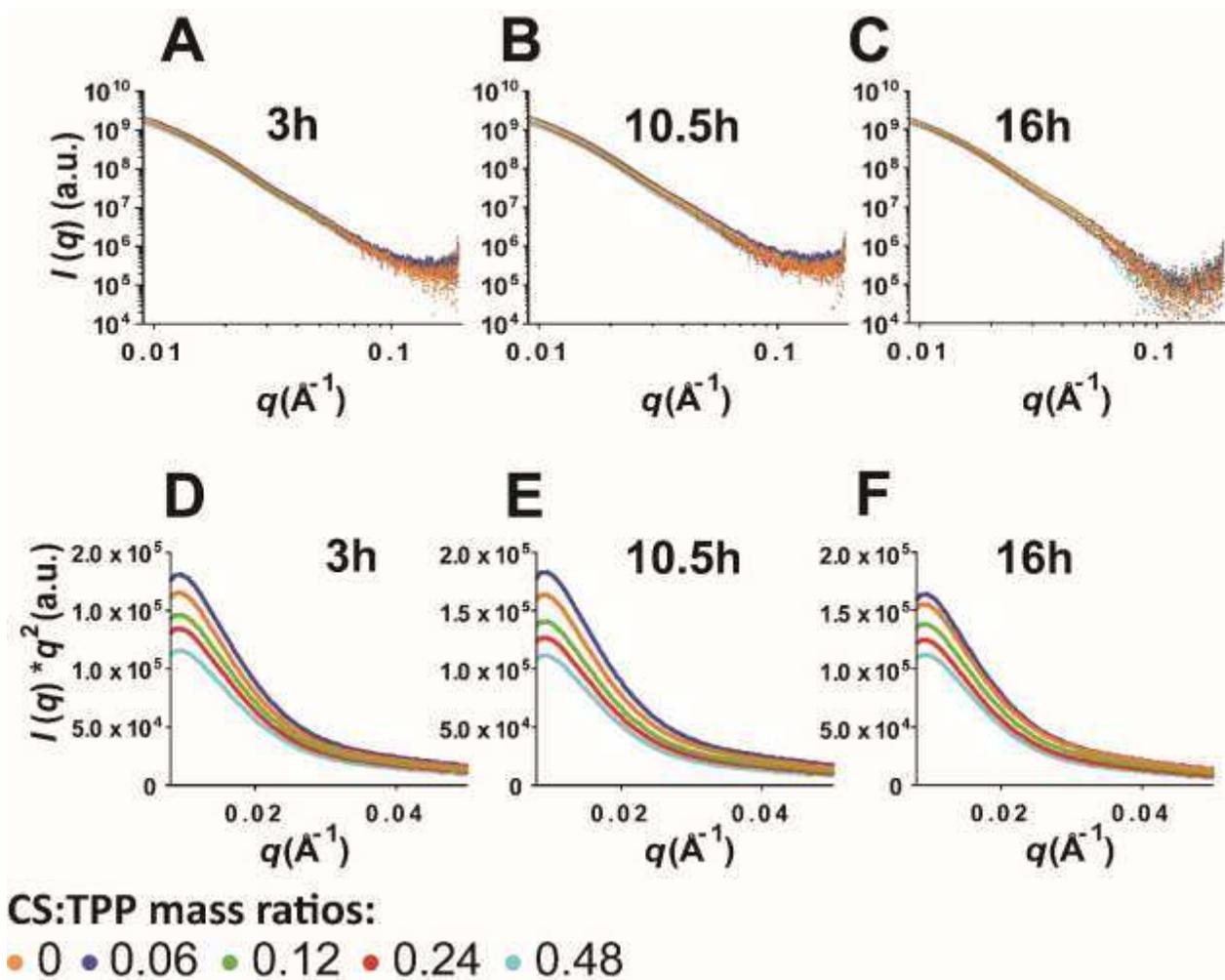
Figure 2. Kratky plots. A-C. SAXS intensity patterns of CC-NPs (1 mg/mL) at varying GNP:CS mass ratios after 3 (A), 10.5 (B) and 16 (C) h of incubation at 37 °C. Data represent the mean of three triplicated treatmens in each condition. For the sake of clarity, no error bars are shown. X-axes, q in Å^{-1}. Y-axes, $I(q)$ in arbitrary units (only shown on the left panel for clarity). D-F. Kratky plots for the curves shown in A-C. Data represent the mean of three replicates. For the sake of clarity, no error bars are shown. X-axes, q in Å^{-1}. Y-axes, $I(q) \cdot q^2$ in arbitrary units (only shown on the left panel for clarity). GNP:CS mass ratios for panels A-F are colour coded as shown at the bottom of the figure.

for CC-NPs with different degrees of GNP crosslinking, after 3, 10.5 and 16 h of incubation, respectively (see also Figure S4). We performed regression analysis in the $1/q^2$ range from 2130 to 879 Å^2, *i.e.* in the q range from 2.1 10^{-2} to 3.4 10^{-2} Å^{-1}. Dashed black lines in Figure 3 A-C show the fitted $I(q)*q^2$ *vs. $1/q^2$* values yielding negative y-axis intercepts, hence suitable to adjustment to the core-shell model (see also Figure S4). Figure 3D represents the evolution of shell thickness over time for the various systems after incubation at 37 ºC, as deduced from Equation 6. As shown in the bar diagram, at early incubation times, all the systems, including the one in the absence of GNP, could be fitted adequately to the core-shell model, with estimated average values of shell thickness ranging from ~40 to 55 Å. However, from 10.5 h of incubation onwards and until the end of the experiment, it was only possible to unambiguously apply the core-shell model to CC-NPs with GNP:CS mass ratios between 0.12 and 0.48 (see Figure S4 and Table S2). Interestingly, low GNP:CS mass ratios (*i.e.* at or below 0.06) ageing for at least 10.5 h at 37 ºC, neither induced the formation of diffuse interphase nor a reduction in the intensity of the peak in the Kratky plots (panels D-F in Figure 2). Thus, there appears to be two steps in NP shell structuration. In the absence of GNP stabilization by crosslinking, an initially present particle shell vanished after extended incubation times (dashed lines in Figure 3D. See also Table S2). In presence of higher amounts of GNP, however, the thickness of the initial shell increased with incubation time (green and yellow bars in Figure 3D). This second phase was both time- and GNP-dependent, reaching a maximum shell thickness of 75.9 ± 20.3 Å after a 16-h incubation, in the case of the 0.48 GNP:CS mass ratio. In addition, for GNP:CS mass ratios greater than 0.06, the intensity of the associated Kratky peaks (Figure 2D-F) decreased relative to the no-GNP control, while shell thickness increased (Figure 3D). Thus, the results presented in Figures 2D-F and 3D might reflect two sides of the same process of structural evolution, in that the reduced contrast factors caused by higher
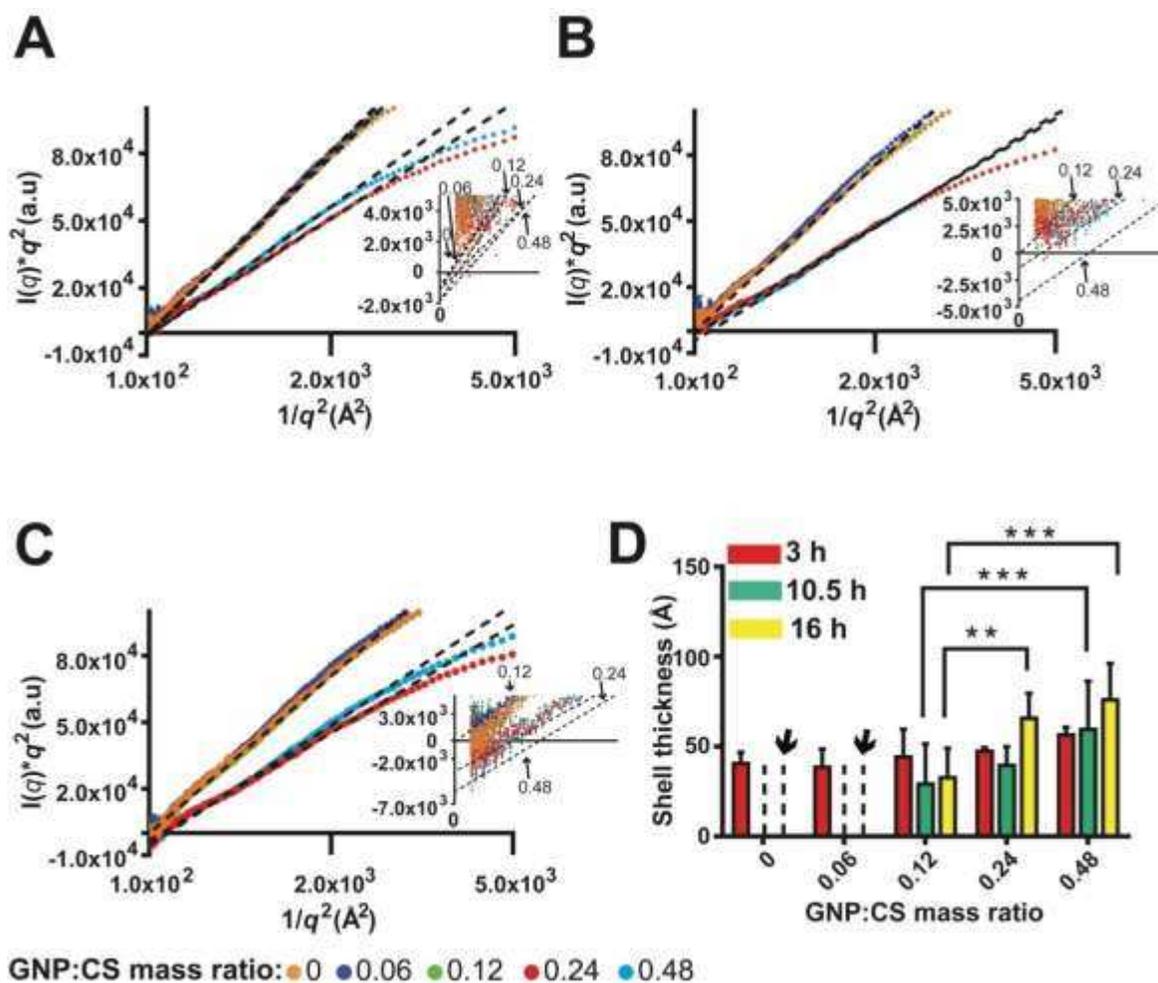
Figure 3. Determination of the width of the diffuse interface of CC-NPs at varying GNP:CS mass ratios. A-C $I(q)q^2$ *vs* $1/q^2$ plots (dotted lines) obtained at the GNP:CS mass ratios indicated by colour key shown at the figure bottom. X-axes, $1/q^2$ in Å^2. Y-axes, $I(q)*q^2$ in arbitrary units. NPs were incubated for 3 (A), 10.5 (B) and 16 (C) h at 37 ºC. To estimate the width of the transition layer, the Porod's asymptotic behavior was studied according to Equation 5 [64], where C and -B are the intercept and slope of the linear, best-fit parameters of the modified Porod treatment (see Equation 5 and 6), respectively. Dashed black lines show the best linear fits from which the slopes were calculated. Data represent the values of a single, representative experiment out of a total of three replicates (but see Figure S4). Only data with linear fits yielding Y-axis intercepts at negative $I(q)*q^2$ values, hence suitable to be described by Equation 6, are shown (but see Table S2 and Figure S4). The $1/q^2$ region ranging from 0 to $1x10^2$ was not shown in main plot for clarity. The insets show a zoomed-in view of the Y-intercept region. Data points lying in the $1/q^2$ region ranging from 0 to 50 were omitted in insets for clarity. The identity of the linear fits is indicated in insets. D. Calculated shell thickness after incubation at 37 ºC according to Equation 6 [64]. Arrowheads indicate ambiguities due to insufficient experimental data (see Table S2 and Figure S4). In such cases, the clear trend displayed by the data represented in Table S2 was used to infer the behavior displayed in this figure. X-axis, GNP:CS mass ratio values, Y-axis: shell thickness in Å. Data represent the average value and standard deviation of the three replicates mentioned above. Statistical comparisons between treatments at different incubation times were made with GraphPad Prism 6 using two-way ANOVA with multiple-comparison Tukey test (** p $\leq$ 0.01; *** p $\leq$ 0.001).

levels of GNP crosslinking could also be linked to the formation of thicker shells during extended incubation, as deduced by the modified Porod law.

Physicochemical characterization of prototype IC-NPs and CC-NPs:

NP isolation via centrifugation followed by resuspension in glycerol has been reported as a critical step in the fabrication of CS-TPP NPs [65]. Prior to isolation, the parent batch of IC-NPs had an average diameter of 150 ± 50 nm and a low PdI of ~0.1-0.2 (Figure 4A and B). Following isolation, IC-NPs were highly sensitive to the process of resuspension and tended to aggregate. This behavior resulted in important differences in the Z-average sizes and PdI values of isolated IC-NPs, relative to their parental counterparts (Figure 4A and B). As a result, isolated IC-NPs were characterized by wider DLS-NIBS size distribution plots, indicating that they possessed much larger average hydrodynamic diameters than those of their parental NPs, *cf.* ~334 nm *vs.* 150 ± 50 nm (lower left panel in Figure 4C). The PdI values increased from ~0.1-0.2 to ~0.3-0.7 (Figure 4B). Notably, the size distribution was highly batch dependent, often displaying multi-modal character and signals of the presence of extremely large particles of unresolvable size (lower right panel in Figure 4C, see also Figure S5). On the contrary, isolated CC-NPs systematically retained the original average diameter and PdI values of their parental NPs (size: 151 ± 7, PdI: 0.1-0.2) (Figure 4A-C). When the average diameter of the individual preparations was considered, isolated CC-NPs were found to be even better behaved than parental IC-NPs (*cf.* panels A and B in Figure S5). Thus, GNP co-crosslinking provides an avenue to circumvent the tendency of IC-NPs to aggregate after isolation, effectively resulting in NPs with a narrow diameter range.

The ζ-potential of isolated IC-NPs and CC-NPs was estimated in two different saline environments, namely 1 mM KCl and 85 mM NaCl. The first saline environment, with low ionic strength and neutral pH, is customarily employed by our group [66-71] and others [72-74] to compare the ζ-

potential values of CS-based NPs. The second saline environment, 85 mM NaCl, is the one chosen for the fabrication of IC-NPs and CC-NPs, as described above. Figure 4D shows the mean ζ-potential of the isolated IC-NPs and CC-NPs in both environments. In 1 mM KCl, IC-NPs displayed a ζ-potential of +25.4 ± 5.5 mV. Under these conditions, covalent crosslinking with GNP slightly reduced the surface charge, yielding a ζ-potential value of +20.1 ± 2.3 mV. The overall reduction in ζ-potential after GNP co-crosslinking of CS-TPP NPs was the expected consequence of the covalent interaction of GNP with CS, yielding secondary amines in the neutral state [38]. The same trend was observed in 85 mM NaCl, although the measured ζ-potential values were considerably lower in this medium, namely +16.4 ± 0.8 mV and +10.5 ± 0.9 mV for IC-NPs and CC-NPs, respectively. Reduction of the ζ-potential at 85 mM NaCl was expected due to increased salt-induced screening of charges at higher ionic strength, together with the known strong dependence of surface charge densities on ionic strength (Debye-Hückel prediction) [13, 56, 75]. Along these lines, Huang and Lapitsky [56] showed that despite the lower ζ-potential observed at higher ionic strength, increased colloidal stability can be achieved, likely due to salt-mediated inhibition of bridging flocculation.

CC-NPs remain stable during incubation in biological medium:

To evaluate the physical stability of IC-NPs and CC-NPs in microbiological assays, we followed the evolution of particle size during incubation in biological medium. To this end, we prepared 1/50 dilutions of IC-NPs and CC-NPs in supplemented M9 minimal medium, pH 6.9 ± 0.05 (see Materials & Methods), incubated the samples at 37 ºC, and recorded the DLS size distributions at specific time points, namely 0, 2, 4 and 6 h. The medium and the incubation conditions were not arbitrary, as they mimic the conditions of a typical bioassay with the *E. coli* biosensor. Our previous experience with IC-NPs had revealed that these NPs are rather unstable in most biological media
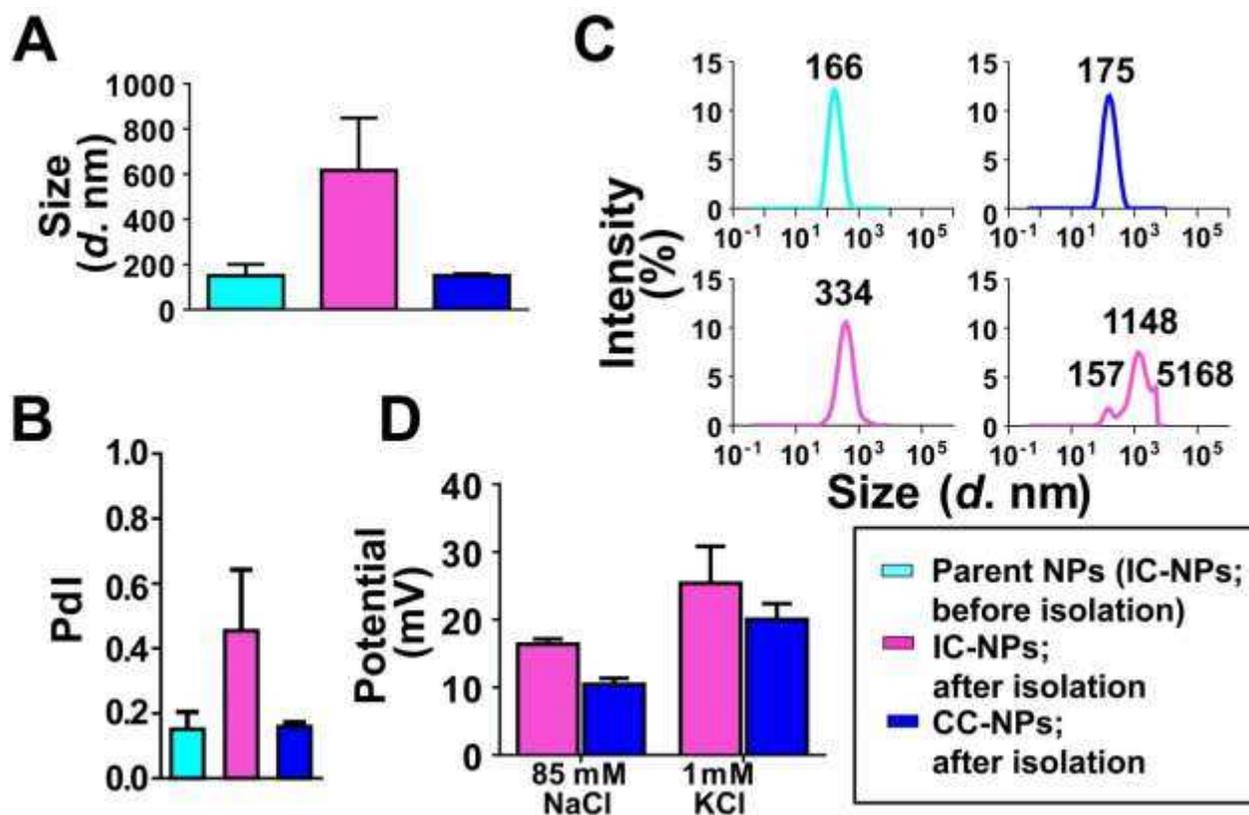
Figure 4. Physico-chemical characterization by DLS-NIBS of the parent IC-NP batch (before isolation) and of isolated IC-NPs and CC-NPs. A. Z-average size (diameter) of NPs. Data represent the average value and standard deviation of six (parent NPs) to nine (isolated IC-NPs and CC-NPs) replicates. For simplicity, labeling has been omitted on X axis but the plotted bars NPs are colour coded as indicated in box. Y-axis, Z-average, NP diameter in nm. B. Mean PdI for the three NP systems of A. X axis and colour coding as in A. Y-axis, average PdI values. Colour coded as in A. C. Representative DLS intensity size (diameter) distribution plots for the three NP systems of A (see also Figure S5). In the case of isolated IC-NPs, two representative plots are shown. Colour coded as in A. X-axis, average diameter in nm. Y-axis DLS intensity in percentage. D. Mean ζ-potential for isolated IC-NPs and CC-NPs in 85 mM NaCl and in 1 mM KCl. Y-axis, average ζ-potential values in mV. X axis and colour coding as in A.

[27]. In addition, other authors have reported precipitation of CS NPs upon mixing with bacterial broth [76]. Not surprisingly, DLS-NIBS analysis revealed that IC-NPs were highly unstable in supplemented M9 minimal medium, as shown by the impossibility of obtaining satisfactory intensity-based size distributions, even at time zero (Figure 5A). However, we did not detect any visible aggregation upon inoculation and incubation of IC-NPs in bacterial broth. Of note, the DLS-NIBS correlograms of IC-NPs in the culture medium showed a delayed decay in the correlation curves characteristic of large particles (Figure 5C). By contrast, CC-NPs were completely stable in M9 minimal medium throughout the duration of the experiment and they showed monomodal size distributions, and monotonic intensity correlation functions up to ~10^3 µs (Figure 5B and D, respectively).

Microbiological assays:

The *E. coli* reporter strain carrying the genetic device BbaT9009 (see Experimental Section) functions as an AHL receiver whose response (GFP expression) can be measured by the emmited fluorescence [77]. We used this strain as a biosensor to analyze the antimicrobial and QQ activity of IC-NPs and CC-NPs.

Evaluation of the antimicrobial and QQ activity of the IC-NPs and CC-NPs:

As a first approach to characterize the bioactivity of IC-NPs and CC-NPs with the *E. coli* fluorescent QS biosensor, we tested the effects of fixed NP concentrations on cell growth kinetics. When growth rates values are considered (Figure 6A and B), a clear antimicrobial effect of both types of NPs is observed. In both cases, dose dependence is conspicuous at low to medium NP concentrations and peters out at higher dosages. The growth curves of Figure 6C and D show that for the two treatments, low NP concentrations (IC-NPs: up to 12.52 µg/mL; and CC-NPs: up to
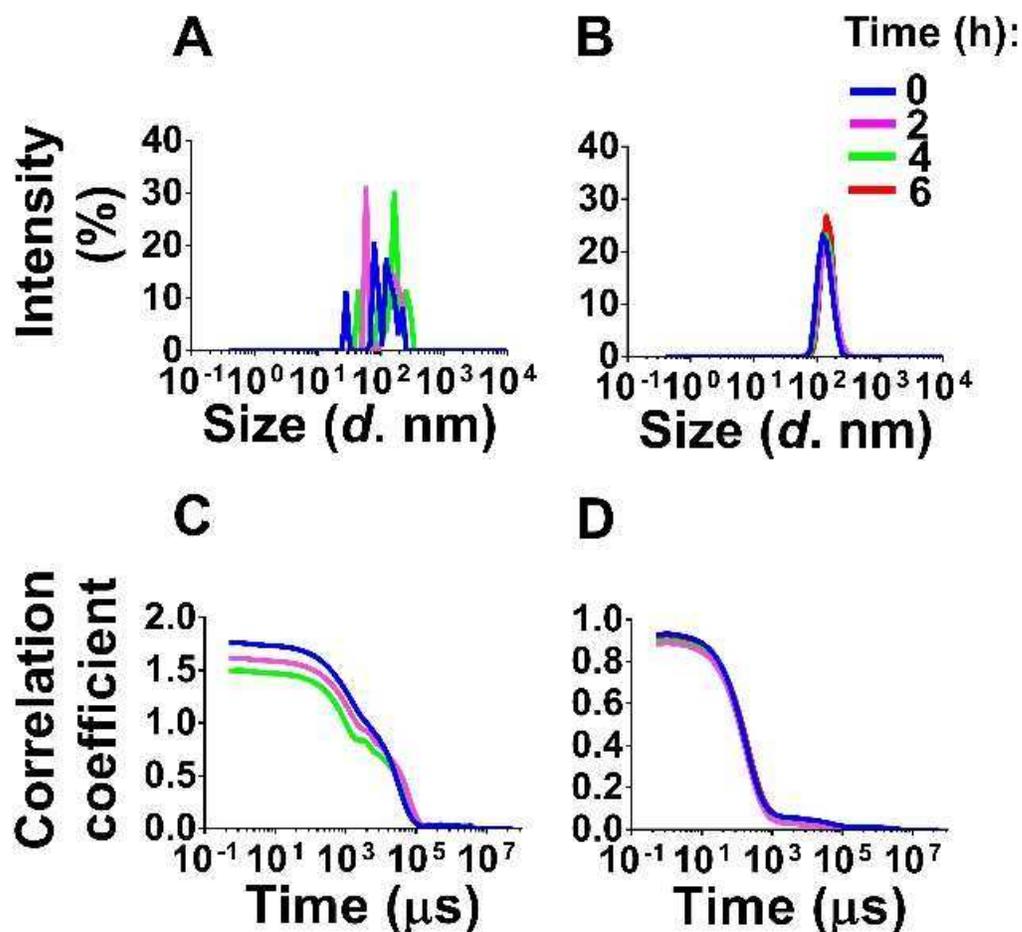
Figure 5. Stability of IC-NPs and CC-NPs in M9 minimal medium. A-B. DLS size distribution plots for IC-NPs (A) and CC-NPs (B). Colour key indicates the incubation time in supplemented M9 minimal medium at 37 ºC. X-axes, average diameter in nm. Y-axes, DLS intensity in percentage. C-D. DLS correlograms of IC-NPs (C) and CC-NPs (D) at different incubation times. X-axes, time in µs. Y-axes, average correlation coefficient. Colour coded as in A-B. Data represent de mean DLS values of three replicates. For the sake of clarity, error bars are not included.

13.16 μg/mL), yielded growth kinetics that were similar to those of controls, despite the clear existence of a slight NP effect (see below). In contrast, treatment with higher NP concentrations resulted in significantly decreased growth rates. Significant experiment-to-experiment variation was evident in these assays, as indicated by the large standard deviations shown in Figure 6C and D. Additional anomalies in the form of "shoulders" were also apparent in some of the curves (downward arrows in Figure 6C and D). For clarity, we show the individual time/OD_{600} traces in Figures S6-S9 (main panels). In the case of IC-NPs, an initial phase of growth can be observed at which the behavior of the treated biosensor cultures was indistinguishable from that of the untreated controls at all IC-NP concentrations (first 100-150 min) (main panels in Figures S6 and S7). Following this phase, OD_{600} traces from treated cultures deviate from those of controls towards lower growth rates (main panels in Figures S6 and S7). At the two lowest IC-NP concentrations, the three biological replicates deviated from the controls to different degrees and displayed sharp anomalies (main panels B and C in Figures S6 and S7), resulting in the shoulders shown in Figure 6C. The presence of anomalies was much more accused in the case of CC-NPs (main panels in Figures S8 and S9). This, together with a much higher degree of experimental variability (*cf.* main panels in Figures S8 and S9), made these growth results much harder to interpret than those of IC-NPs.

Next, we attempted to monitor the toxicity of our NPs by means of a survival assay. Since our previous experience with CS nanocapsules showed that they could bind to bacterial cells and promote cell aggregation [50], we decided that a simple colony-counting method could fail to provide a reliable estimate of the fraction of viable cells after treatment with our NPS. Instead, we decided to monitor the growth of the fraction of viable cells remaining after exposure to the NPs [78, 79]. With this in mind, we pre-treated the cells for 5 h with various doses of IC-NPs and CC-

NPs in M9 minimal medium, after which the cells were diluted 1:10 in NP-free, fresh broth and incubated for a further 5 h. We then plotted the OD_{600} values in terms of percentage of cell viability *vs*. NP concentration and fitted the resulting curves to a non-linear dose-response function to estimate the IC_{50} values for both IC-NPs and CC-NPs. As shown in Figure 6E, IC-NPs showed an IC_{50} value (IC_{50}= 16.8 µg/mL) that was two-fold lower than that of CC-NPs (IC_{50}= 34.9 µg/mL). The higher toxicity of IC-NPs relative to CC-NPs indicates that GNP co-crosslinking reduces the antimicrobial activity of the former NPs.

Next, we analyzed the QQ activity of our NPs by measuring their ability to interfere with the biosensor's QS-induced fluorescence (see Experimental Methods). Despite the noted differences in the apparent growth rates, an overall strong reduction of end-point, OD_{600}-normalized fluorescence (Fl/OD_{600}) was clear for most NP concentrations (Figure 7A and B). The effect was significantly more pronounced for IC-NPs than for CC-NPs (*cf.* Figure 7A and B). Panels C-F of Figure 7 show the average Fl/OD_{600} traces from two independent experiments for both IC-NPs and CC-NPs (the individual traces are shown in insets in Figures S6-S9). In keeping with the endpoint results, a strong reduction of normalized fluorescence was observed at all concentrations of IC-NPs (Figure 7C and D). Notably, maximal Fl/OD_{600} reduction was achieved at the lowest NP concentration, and no additional reduction could be afforded by higher concentrations (Figures 7C and D). Moreover, despite the noted presence of large standard deviations in OD_{600} values, the error associated to Fl/OD_{600} in the same experiments was much lower (*cf.* Figure 6C to panels C and D of Figure 7), supporting the existence of a strong QQ effect mediated by these NPs. Again, large experimental differences in the case of CC-NPs, made it difficult to interpret the Fl/OD_{600} results at all NP concentrations, except for the highest (Figure 7E and F). These results prompted us to disregard CC-NPs as reliable QQ-promoting NPs.

Importantly, the fluorescence measurements used in the QQ bioassays have been normalized to cell density (Fl/OD_{600}) [80, 81], meaning that a simple interpretation in which the observed antimicrobial effect might be responsible for the fluorescence decrease cannot hold. To explain the sharp reduction of normalized Fl/OD_{600} observed at all concentrations of IC-NPs, one must claim that the decrease in fluorescence must be of greater magnitude than the OD_{600} drop. The presence of anomalies in the form of "shoulders" in some of the growth curves (downward arrows in Figure 6C and D and Figures S6-S9) is also relevant in this regard. While we have not explored further these growth anomalies in the context of the NPs described in this manuscript, similar irregularities were described by our group in the case of CS nanocapsules [50]. The effect was due to the so called "stoichiometric ratio" of nanocapsules/bacteria, *i.e.* a particular time during growth in the presence of these particles, at which the electrical charge of the bacterial cell wall was compensated by bound nanocapsules, resulting in bacterial aggregation [50]. Hence, it is possible that part of what we interpreted here as growth reduction might have been simply caused by anomalies in the OD_{600} readings due to cell aggregation [82] and that the antimicrobial effect measured in Figure 6E might have been overestimated.
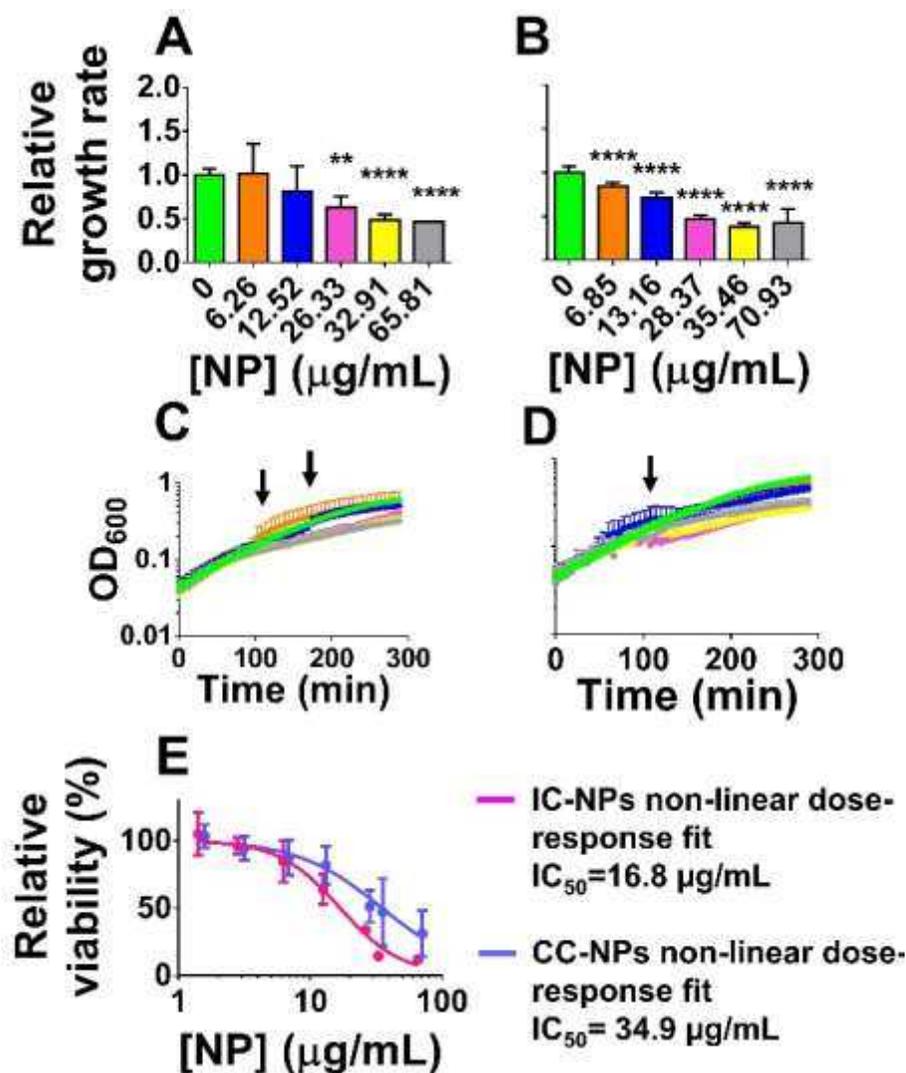
Figure 6. Effect of NP treatment on the growth of the *E. coli* biosensor. A-B. Effect of treatment with IC-NPs (A) and CC-NPs (B) on the biosensor's growth rate, relative to untreated controls. X-axes, NP concentration in μg/mL, determined as described in Materials & Methods. Y-axes, average relative growth rate values. P values are labeled as follows: ** $p \leq 0.01$, *** $p \leq 0.001$, and **** $p \leq 0.0001$. C-D. OD_{600} plots of the *E. coli* biosensor treated for 300 min with varying doses of IC-NPs (C) and CC-NPs (D). Downward arrows in C and D show growth anomalies in the form of "shoulders" observed at some NP concentrations. Data represent the mean and standard deviation of two independent experiments with three biological replicates each. For the sake of clarity, only one-sided error bars are shown. Curves are colour coded to the NP concentrations shown in A and B. X-axis, time in minutes. Y-axis, average OD_{600} values in log scale. E. Viability (%) of *E. coli* cultures pre-treated with IC-NPs and CC-NPs relative to that of control cells, as a function of NP concentration (see Experimental Section). Dots represent the experimental data, and solid lines represent the best-fit to the non-linear dose-response function (GraphPad version 6.00, GraphPad Software, La Jolla California USA), used to calculate the IC_{50} values for the two types of NPs (see Experimental Section). Data represent the mean and standard deviation of two independent experiments with three biological replicates each. X-axis: NP concentration in μg/mL. Y-axis: average relative viability in percentage.
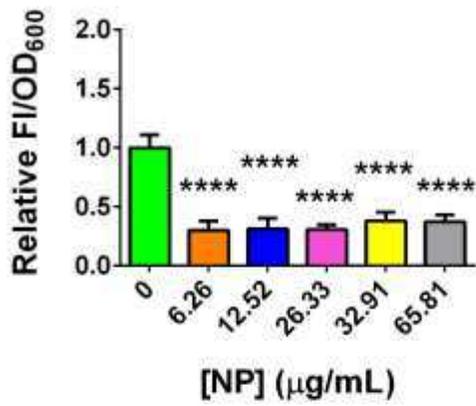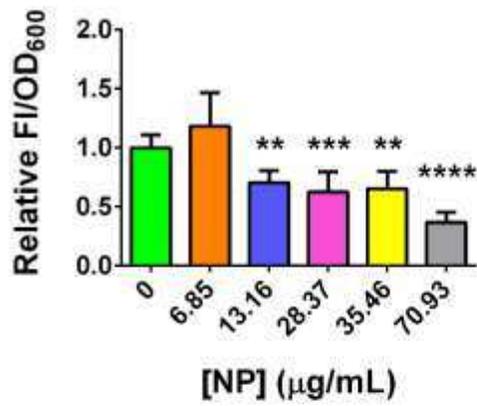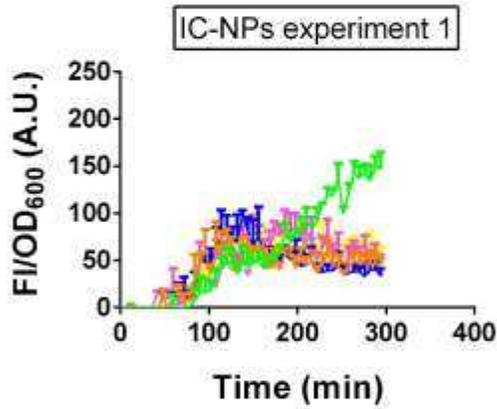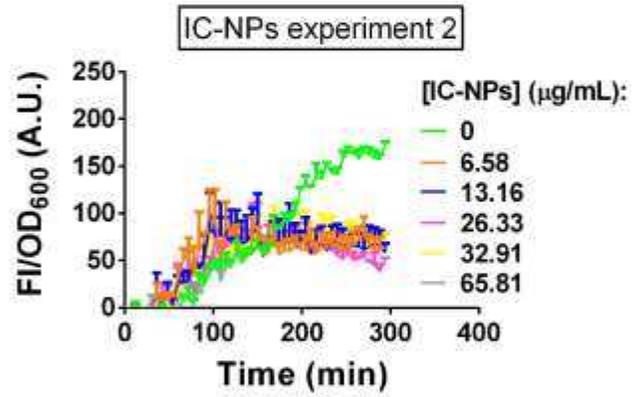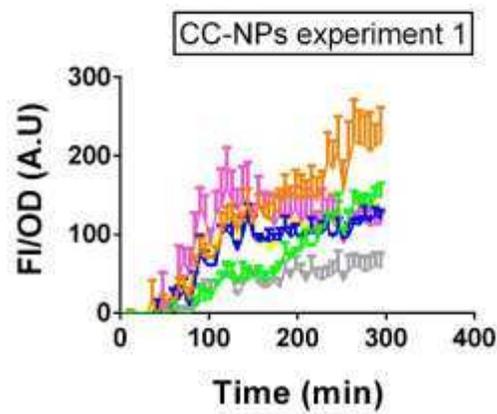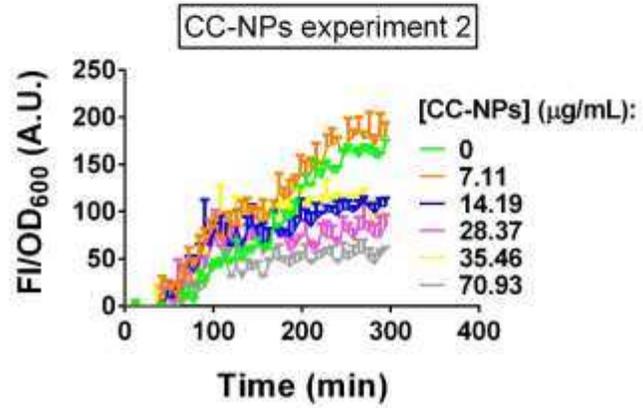
Figure 7. Effect of treatment with IC-NPs and CC-NPs on the QS-based fluorescent response of the *E. coli* biosensor. A-B. End-point Fl/OD$_{600}$ response of the *E. coli* biosensor after treatment with various concentrations of IC-NPs (A) and CC-NPs (B), relative to that of control cells. Data represent the mean and standard deviation of two independent experiments with three biological replicates each. P values are labeled as follows: ** p $\leq$ 0.01; *** p $\leq$ 0.001; **** p $\leq$ 0.0001. X-axes, NP concentration in µg/mL. Y-axes, average relative FL/OD$_{600}$ values. C-F. Effect of various concentrations of IC-NPs (C, D) and CC-NPs (E, F) on the FL/OD$_{600}$ response of the *E. coli* biosensor in two independent experiments (C, D and E, F, respectively). Data represent the average and standard deviations of three biological replicates per experiment. For the sake of clarity, only one-sided error bars are shown. The traces of C and E are colour coded as in D and F, respectively. X axes: Time in minutes. Y axes: Fl/OD$_{600}$ in arbitrary units.

DISCUSSION

Despite the initial high expectations for CS micro- and nano-particles crosslinked with TPP, their colloidal stability under biologically relevant conditions remains a major shortcoming towards their wider use as broad-spectrum bio-nanomaterials [16, 83-86]. Indeed, in our study, IC-NPs had a tendency to increase in size and polydispersity after isolation by centrifugation (Figure 4). This undesired attribute of IC-NPs was further complicated by their batch-dependent behavior (Figure S5). The tendency of TPP-crosslinked CS NPs to aggregate after centrifugation is well known [65]. For this reason, the standard fabrication method used in our group and by others includes the use of a glycerol bed during centrifugation to avoid aggregation [87, 88]. Other laboratories have resolved this issue by resorting to aggressive methods of aggregate disruption, such as ultrasonication [89, 90]. Aggregation could be due to the reported tendency of unmodified chitosan particles to produce vortex-resistant aggregates as a result of strong inter- and intra-molecular hydrogen bonding [54, 91]. Tanaka et al. [54] also mentioned the existence of strong hydrophobic interactions responsible for the aggregation of CS.

In contrast to IC-NPs, CC-NPs tolerated well their manipulation during the process of centrifugation and resuspension (Figure 4). Covalent crosslinking with GNP could prevent the formation of undesired hydrogen bonds and/or hydrophobic interactions, thus, reducing the

tendency of IC-NPs to aggregate. Regardless of the mechanism, GNP crosslinking succeeded in providing a formulation capable of producing robust NPs that can be used as a chassis for down-the-line applications.

We examined the effect of GNP on the physical structure of the CC-NPs at the particle's surface-solvent boundary by using a modified Porod law accounting for the existence of a core-shell structure [63]. This made it possible to evaluate the shell thickness of our NPs in the 1-50 nm resolution range (Figure 3). We observed that the behaviour of all the NP systems, even the ones lacking GNP, could be adequately fitted to the core-shell model at early incubation times at 37 ºC (Figure 3D). This is in agreement with previous reports on the core-shell structure of TPP-crosslinked NPs imaged by transmission electron microscopy (TEM), showing differential structure density between the outer and inner NP boundaries [16, 92]. In contrast, at 37 °C and at incubation times longer than 10.5 h, only NPs formed with GNP:CS mass ratios between 0.12 and 0.48 were successfully modelled by the core-shell model (Figure 3D). This effect was clearly dependent on the incubation step, as IC-NPs are stable at the storage temperature (5 ºC) [16]. The disruption of the GNP-independent core-shell structure of IC-NPs at physiological temperature might imply that the organization of the external boundaries of these NPs (and of insufficiently GNP-crosslinked CC-NPs, see 0.06 GNP:CS mass ratio in Figure 3D), either fluctuates more extensively or suffers from instability upon long incubation at 37 °C. Indeed, we have shown evidence of noticeable reduction in shell thickness at short to medium incubation times, followed by a consistent increase in thickness at longer times (Figure 3D). The shrinkage at low incubation times might be related to restructuring, upon covalent crosslinking with GNP, of the initially swollen and loose, outermost CS strands, into a more compacted conformation. On the other hand, the increase in shell thickness observed at longer times appears to be consistent with additional macromolecular organization of the multi-bridged CS-GNP crosslinked networks, a process that is

known to occur at a slow rate in the later stages of chemical crosslinking with GNP [44, 45]. In such scenario for the evolution of the structure of CS:TPP crosslinked nanoparticles, it becomes clear that the crosslinking reaction of GNP strongly impacts the surface of CC-NPs, relative to their GNP-non-crosslinked counterparts. Other authors have also reported evidence of enhanced mechanical strength, improved chemical stability and reduced swelling behaviour of core-shelled, CS-based microcapsules covalently crosslinked at GNP:CS mass ratios around 0.1 [39]. Our discovery that GNP co-crosslinking of IC-NPs led to the stabilization of a pre-existing, but labile, core-shell structure, likely explains the improved physico-chemical properties displayed by CC-NPs.

An unexpected result during the characterization of our NPs was the discrepancy between DLS-NIBS analysis, which resulted in particles with hydrodynamic diameters of ~200 nm (Figure 1F), and Kratky-plot and Porod-Debye plot analysis of SAXS data, which yielded an Rg of ~ 17 nm (Figure 2D-F). While there might exist a subset of CC-NPs in our preparations with diameters significantly smaller than the DLS-determined value of ~200 nm, the consistent behaviour displayed during DLS-NIBS (Figure 5) indicates that smaller particles, if existing, are expected to be minoritarian. We prefer to explain the apparent discrepancy between SAXS and DLS-NIBS in the context of the "raspberry-like" model of NP ultrastructure proposed by Huang and Lapitsky for TPP-crosslinked CS-NPs [93]. Accordingly, we propose that the size of our NPs results from the aggregation of primary, smaller nanoparticles into larger objects with sizes ~ 200 nm.

The superior physico-chemical features of CC-NPs, together with their higher stability under biological conditions (Figure 5) and lower toxicity (Figure 6) makes these NPs better suited for microbiological work than IC-NPs. For example, CC-NPs constitute a promising chassis for the design of smart drug delivery nanocarriers under conditions in which QQ is not desired. Since the suitability of GNP crosslinked, CS-based matrices for drug delivery and controlled release has been

amply demonstrated [32, 35-40, 94-96], the results presented here are in line with the existence of a high potential for our CC-NPs to bear multifunctional structures, respond to external stimuli, and/or to be combined with adjuvant biomolecules.

CS has recently been proposed as a new generation antimicrobial with the capacity to control a broad spectrum of microorganisms, including antibiotic resistant pathogens [48, 49, 97]. Raw CS has been shown to interfere with QS responses and biofilm formation in various bacterial pathogens [48, 49]. However, the potential of CS-based nanomaterials to directly inhibit QS has only recently been studied. Our group has shown that CS nanocapsules can bind to bacterial cells, promote cell aggregation and attenuate the QS response of a model biosensor [50]. Here, we have also shown that both IC-NPs and CC-NPs exhibit antimicrobial and QQ-like properties, albeit in the case of CC-NPs, consistent QQ activity is only observed at high NP concentrations (Figures 6 and 7). The results of Figure 6 and 7 are in agreement with the existence of two different effects of low-to-medium concentrations of IC-NPs on the biosensor, namely a slight antimicrobial effect and a much stronger QQ effect. The surprisingly strong and stable QQ activity of IC-NPs stands in stark contrast to their erratic physicochemical properties. Thus, this work, together with our previous report [50], indicate that certain CS-based nanomaterials, such as IC-NPs or CS nanocapsules, satisfactorily maintain the QQ activity of free CS. This occurs, despite the vast size of these nanomaterials, in comparison to CS, and the important structural differences arising from their formulations. Thus, IC-NPs could serve as the chassis for microbiologically relevant CS-NPs capable to interfere with QS. Further work will be required to fully separate the influence of bacterial aggregation resulting from the "stoichiometric effect" [50] from the true antimicrobial and QQ activities of IC-NPs. This will likely require a deep understanding of the nature of the interaction between IC-NPs and the cell wall. The results presented here are also clear about the requirement of future efforts towards improving the physicochemical stability of IC-NPs. As such,

IC-NPs can be considered as the starting point for the fabrication of NPs with the ability to combine QQ with other functions of interest, thus, providing these particles with the ability to directly alter the normal growth kinetics of bacterial populations in yet unforeseen manners.

Finally, the comparison of IC-NPs and CC-NPs presented here has far reaching consequences for the future design of CS-NPs. Our SAXS analysis indicating the stabilization of a labile core-shell structure upon GNP crosslinking, together with the widely different properties exhibited by IC-NPs and CC-NPs, strongly suggest that modulating the features of the shell during crosslinking could lead to new types of NPs with a variety of interesting properties.

CONCLUSION

TPP- and GNP-crosslinked CS nanosystems have been the subject of numerous previous studies. However, the relationship between the nanosystem's ultrastructure and its final properties and potential applications has not been studied in detail. After comparing the physicochemical properties and the biological performance of two related types of CS nanosystems, namely ionically (TPP) crosslinked IC-NPs and dually (TPP+GNP) crosslinked CC-NPs, we observed that, despite the similarities in their composition, both systems had widely different behaviors. CC-NPs showed enhanced colloidal stability during the process of centrifugation and resuspension and upon incubation in microbiological medium, maintaining their average diameter in the range of ~200 nm In contrast, IC-NPs aggregated and were highly unstable in these conditions. Regarding their biological performance, CC-NPs displayed half of the toxicity of IC-NPs (IC_{50}=34.9 µg/mL *vs*. 16.8 µg/mL). On the other hand, the QQ activity of CC-NPs was much lower than that of IC-NPs which had strong QQ activity even at the lowest doses tested (6.58 µg/mL).

By high-brilliance synchrotron SAXS analysis, we were able to elucidate important structural differences between IC-NPs and CC-NPs, namely the long-term stabilization of a pre-existing, but

labile core-shell structure upon crosslinking with GNP in CC-NPs. Thus, the improved colloidal stability and the different biological properties of these NPs appear to arise from the presence of such a core-shell structure. Thus, our work underscores the influence of the NP's ultrastructure on the colloidal and functional (biological) properties of the final product.

This work, together with our previous report [82] indicate that certain CS-based nanomaterials, such as IC-NPs, satisfactorily maintain the QQ activity of free CS, despite their vast size (in comparison to CS). Thus, IC-NPs could serve as the chassis for microbiologically relevant CS-NPs capable to interfere with QS. In contrast, the superior physico-chemical features of CC-NPs, together with their higher stability under biological conditions and lower toxicity makes these NPs better suited for microbiological work than IC-NPs. For example, CC-NPs constitute a promising chassis for the design of smart drug delivery nanocarriers under conditions in which QQ is not desired.

REFERENCES

[1] S. Berkner, S. Konradi, J. Schonfeld, EMBO Rep. 15 (2014) 740. doi:10.15252/embr.201438978 [doi].

[2] D.J. Payne, L.F. Miller, D. Findlay, J. Anderson, L. Marks, Philos Trans R Soc Lond B Biol Sci. 370 (2015) 20140086. doi:10.1098/rstb.2014.0086 [doi].

[3] S.T. Rutherford, B.L. Bassler, Cold Spring Harb Perspect Med. 2 (2012) 10.1101/cshperspect.a012427. doi:10.1101/cshperspect.a012427 [doi].

[4] N. Mangwani, H.R. Dash, A. Chauhan, S. Das, J Mol Microbiol Biotechnol. 22 (2012) 215. doi:10.1159/000341847.

[5] W.L. Ng, B.L. Bassler, Annu Rev Genet. 43 (2009) 197. doi:10.1146/annurev-genet-102108-134304 [doi].

[6] W.C. Fuqua, S.C. Winans, E.P. Greenberg, J Bacteriol. 176 (1994) 269. doi:10.1128/jb.176.2.269-275.1994 [doi].

[7] C. Fuqua, E.P. Greenberg, Nat Rev Mol Cell Biol. 3 (2002) 685. doi:10.1038/nrm907 [doi].

[8] D.G. Davies, M.R. Parsek, J.P. Pearson, B.H. Iglewski, J.W. Costerton, E.P. Greenberg, Science. 280 (1998) 295. doi:10.1126/science.280.5361.295 [doi].

[9] Y.H. Li, X. Tian, Sensors (Basel). 12 (2012) 2519. doi:10.3390/s120302519 [doi].

[10] B. LaSarre, M.J. Federle, Microbiol Mol Biol Rev. 77 (2013) 73. doi:10.1128/MMBR.00046-12 [doi].

[11] T. Defoirdt, Trends Microbiol. 26 (2018) 313. doi:S0966-842X(17)30232-9 [pii].

[12] M. Dash, F. Chiellini, R.M. Ottenbrite, E. Chiellini, Progress in Polymer Science. 36 (8) (2011) 981.

[13] H. Jonassen, A. Kjøniksen, M. Hiorth, Colloid Polym Sci. 290 (2012) 919.

[14] J. Berger, M. Reist, J.M. Mayer, O. Felt, N.A. Peppas, R. Gurny, Eur J Pharm Biopharm. 57 (2004) 19. doi:S0939641103001619 [pii].

[15] P. Calvo, C. Remuñán-López, J.L. Vila-Jato, M.J. Alonso, J Appl Polym Sci. 63 (1998) 125.

[16] H. Liu, C. Gao, Polym Adv Technol. 20 (2009) 613. doi:10.1002/pat.1306.

[17] X. Zhang, S. Malhotra, M. Molina, R. Haag, Chem Soc Rev. 44 (2015) 1948. doi:10.1039/c4cs00341a [doi].

[18] A. Grenha, J Drug Target. 20 (2012) 291. doi:10.3109/1061186X.2011.654121 [doi].

[19] I.S. Tavares, A.L. Caroni, A.A. Dantas Neto, M.R. Pereira, J.L. Fonseca, Colloids Surf B Biointerfaces. 90 (2012) 254. doi:10.1016/j.colsurfb.2011.10.025 [doi].

[20] Z. Liu, Y. Jiao, Y. Wang, C. Zhou, Z. Zhang, Advanced Drug Delivery Reviews. 60 (2008) 1650. doi:https://doi.org/10.1016/j.addr.2008.09.001.

[21] M. Hamidi, A. Azadi, P. Rafiei, Adv Drug Deliv Rev. 60 (2008) 1638. doi:10.1016/j.addr.2008.08.002 [doi].

[22] M. Garcia-Fuentes, M.J. Alonso, J Control Release. 161 (2012) 496. doi:10.1016/j.jconrel.2012.03.017 [doi].

[23] M.A. Elgadir, M.S. Uddin, S. Ferdosh, A. Adam, A.J.K. Chowdhury, M.Z.I. Sarker, J Food Drug Anal. 23 (2015) 619. doi:S1021-9498(14)00141-0 [pii].

[24] X. Fei Liu, Y. Lin Guan, D. Zhi Yang, Z. Li, K. De Yao, J Appl Polym Sci. 79 (2001) 1324. doi:10.1002/1097-4628(20010214)79:7<1324::AID-APP210>3.0.CO;2-L.

[25] Q. Gan, T. Wang, C. Cochrane, P. McCarron, Colloids and Surfaces B: Biointerfaces. 44 (2005) 65. doi:https://doi.org/10.1016/j.colsurfb.2005.06.001.

[26] V. Kamat, D. Bodas, K. Paknikar, Sci Rep. 6 (2016) 22260. doi:10.1038/srep22260 [doi].

[27] F.M. Goycoolea, F. Brunel, N.E. Gueddari, A. Coggiola, G. Lollo, B.M. Moerschbacher, C. Remunan-Lopez, T. Delair, A. Domard, M.J. Alonso, Macromol Biosci. 16 (2016) 1873. doi:10.1002/mabi.201600298 [doi].

[28] R.A. Muzzarelli, M. El Mehtedi, C. Bottegoni, A. Aquili, A. Gigante, Mar Drugs. 13 (2015) 7314. doi:10.3390/md13127068 [doi].

[29] L. Bi, Z. Cao, Y. Hu, Y. Song, L. Yu, B. Yang, J. Mu, Z. Huang, Y. Han, J Mater Sci: Mater Med. 22: (2011) 51.

[30] M.J. Moura, M.M. Figueiredo, M.H. Gil, Biomacromolecules. 8 (2007) 3823. doi:10.1021/bm700762w [doi].

[31] T.K. Giri, A. Thakur, A. Alexander, Ajazuddin, H. Badwaik, D.K. Tripathi, Acta Pharmaceutica Sinica B. 2 (2012) 439. doi:https://doi.org/10.1016/j.apsb.2012.07.004.

[32] Y. Lin, S. Tsai, C. Lai, C. Lee, Z.S. He, G. Tseng, Biomaterials. 34 (2013) 4466. doi:https://doi.org/10.1016/j.biomaterials.2013.02.028.

[33] Y. Zhang, Y. Thomas, E. Kim, G.F. Payne, J Phys Chem B. 116 (2012) 1579. doi:10.1021/jp210043w [doi].

[34] M.J. Moura, H. Faneca, M.P. Lima, M.H. Gil, M.M. Figueiredo, Biomacromolecules. 12 (2011) 3275. doi:10.1021/bm200731x [doi].

[35] Y. Yuan, B.M. Chesnutt, G. Utturkar, W.O. Haggard, Y. Yang, J.L. Ong, J.D. Bumgardner, Carbohydrate Polymers. 68 (2007) 561. doi:https://doi.org/10.1016/j.carbpol.2006.10.023.

[36] M.P. Klein, C.R. Hackenhaar, A.S.G. Lorenzoni, R.C. Rodrigues, T.M.H. Costa, J.L. Ninow, P.F. Hertz, Carbohydrate Polymers. 137 (2016) 184. doi:https://doi.org/10.1016/j.carbpol.2015.10.069.

[37] X. Song, H. Wu, S. Li, Y. Wang, X. Ma, M. Tan, Biomacromolecules. 16 (2015) 2080. doi:10.1021/acs.biomac.5b00511 [doi].

[38] R. Harris, E. Lecumberri, A. Heras, Mar Drugs. 8 (2010) 1750. doi:10.3390/md8061750 [doi].

[39] H. Chen, W. Ouyang, C. Martoni, S. Prakash, International Journal of Polymer Science. 2009 (2009) 1.

[40] B.M. Espinosa-Garcia, W.M. Arguelles-Monal, J. Hernandez, L. Felix-Valenzuela, N. Acosta, F.M. Goycoolea, Biomacromolecules. 8 (2007) 3355. doi:10.1021/bm700458a [doi].

[41] C.A. Pinto, K.K. Saripella, N.C. Loka, S.H. Neau, Journal of Pharmaceutical Sciences. 107 (2018) 1063. doi:https://doi.org/10.1016/j.xphs.2017.11.018.

[42] J.M. Alonso, F.M. Goycoolea, I. Higuera-Ciapara, (2008) 644. doi:https://doi.org/10.1533/9781845694814.5.644.

[43] X.Z. Shu, K.J. Zhu, International Journal of Pharmaceutics. 201 (2000) 51. doi:https://doi.org/10.1016/S0378-5173(00)00403-8.

[44] M.F. Butler, Y. Ng, P.D.A. Pudney, J Polym Sci A Polym Chem. 41 (2003) 3941. doi:10.1002/pola.10960.

[45] F. Mi, H. Sung, S. Shyu, J Polym Sci A Polym Chem. 38 (2000) 2804. doi:10.1002/1099-0518(20000801)38:15<2804::AID-POLA210>3.0.CO;2-Y.

[46] R.A.A. Muzzarelli, Carbohydrate Polymers. 77 (2009) 1. doi:https://doi.org/10.1016/j.carbpol.2009.01.016.

[47] S.N. Mikhailov, A.N. Zakharova, M.S. Drenichev, A.V. Ershov, M.A. Kasatkina, L.V. Vladimirov, V.V. Novikov, N.R. Kildeeva, Nucleosides Nucleotides Nucleic Acids. 35 (2016) 114. doi:10.1080/15257770.2015.1114132 [doi].

[48] L. Cobrado, M.M. Azevedo, A. Silva-Dias, J.P. Ramos, C. Pina-Vaz, A.G. Rodrigues, J Antimicrob Chemother. 67 (2012) 1159. doi:10.1093/jac/dks007 [doi].

[49] E.M. Costa, S. Silva, C. Pina, F.K. Tavaria, M. Pintado, SOJ Microbiol Infect Dis. 2 (2014) 1.

[50] X. Qin, C. Engwer, S. Desai, C. Vila-Sanjurjo, F.M. Goycoolea, Colloids and Surfaces B: Biointerfaces. 149 (2017) 358. doi:https://doi.org/10.1016/j.colsurfb.2016.10.031.

[51] I. Dmour, M.O. Taha, International Journal of Pharmaceutics. 529 (2017) 15. doi:https://doi.org/10.1016/j.ijpharm.2017.06.061.

[52] J. Shang, X. Gao, Chem Soc Rev. 43 (2014) 7267. doi:10.1039/c4cs00128a [doi].

[53] K.M.C. Tjorve, E. Tjorve, PLoS One. 12 (2017) e0178691. doi:10.1371/journal.pone.0178691 [doi].

[54] K. Tanaka, K. Nishida, B. Gabrys, M. J. Lawrence, T. Kanaya, FIBER. 70 (2014) 225. doi:10.2115/fiber.70.225.

[55] M.L. Tsaih, R.H. Chen, International Journal of Biological Macromolecules. 20 (1997) 233. doi:https://doi.org/10.1016/S0141-8130(97)01165-3.

[56] Y. Huang, Y. Lapitsky, Langmuir. 27 (2011) 10392. doi:10.1021/la201194a [doi].

[57] S. Sreekumar, F.M. Goycoolea, B.M. Moerschbacher, G.R. Rivera-Rodriguez, Sci Rep. 8 (2018) 4695. doi:10.1038/s41598-018-23064-4 [doi].

[58] F.M. Goycoolea, G. Lollo, C. Remunan-Lopez, F. Quaglia, M.J. Alonso, Biomacromolecules. 10 (2009) 1736. doi:10.1021/bm9001377 [doi].

[59] M. Rinaudo, G. Pavlov, J. Desbrières, Int J Polym Anal Charact. 5 (1998) 267.

[60] M. Chalal, F. Ehrburger-Dolle, I. Morfin, F. Bley, M.-. Aguilar de Armas, M.-. López Donaire, J. San Roman, N. Bölgen, E. Pişkin, O. Ziane, R. Casalegno, Macromolecules. 43 (2010) 2009.

[61] N.T. Qazvini, S. Bolisetty, J. Adamcik, R. Mezzenga, Biomacromolecules. 13 (2012) 2136.

[62] S. Popa-Nita, C. Rochas, L. David, A. Domard, Langmuir. 25 (2009) 6460.

[63] M.-. Kim, J Appl Crystallogr. 37 (2004) 643.

[64] A. Drogoz, S. Munier, B. Verrier, L. David, A. Domard, T. Delair, Biomacromolecules. 9 (2008) 583.

[65] E.L.S. Carvalho, A. Grenha, C. Remuñán-López, M.J. Alonso, B. Seijo, Methods in Enzymology. 465 (2009) 289. doi:https://doi.org/10.1016/S0076-6879(09)65015-1.

[66] T. Mengoni, M. Adrian, S. Pereira, B. Santos-Carballal, M. Kaiser, F.M. Goycoolea, Pharmaceutics. 9 (2017) 10.3390/pharmaceutics9040056. doi:E56 [pii].

[67] M. Kaiser, B. Kirsch, H. Hauser, D. Schneider, I. Seuss-Baum, F.M. Goycoolea, PLoS One. 10 (2015) e0141017. doi:10.1371/journal.pone.0141017 [doi].

[68] M. Alonso-Sande, M. Cuña, C. Remuñán-López, D. Teijeiro-Osorio, J.L. Alonso-Lebrero, M.J. Alonso, Macromolecules. 39 (2006) 4152.

[69] H. Thanh Nguyen, F.M. Goycoolea, Molecules. 22 (2017) 1975.

[70] Y. Parajo, I. D'Angelo, A. Welle, M. Garcia-Fuentes, M.J. Alonso, Drug Deliv. 17 (2010) 596. doi:10.3109/10717544.2010.509357 [doi].

[71] M. Peleteiro, E. Presas, J.V. Gonzalez-Aramundiz, B. Sanchez-Correa, R. Simon-Vazquez, N. Csaba, M.J. Alonso, A. Gonzalez-Fernandez, Front Immunol. 9 (2018) 791. doi:10.3389/fimmu.2018.00791 [doi].

[72] L. Bessa Prado, S. Cares Huber, A. Barnabé, F. Dutra, S. Bassora, D. Souza Paixão, N. Duran, J.C. Annichino-Bizzacchi, Journal of Nanotechnology. 2017 (2017) 1.

[73] B. Boonyo, H.E. Junginger, N. Waranuch, A. Polnok, T. Pitaksuteepong, Journal of Metals, Materials and Minerals. 18 (2008) 59.

[74] S.A. Bucarey, M. Pujol, J. Poblete, I. Nunez, C.V. Tapia, A. Neira-Carrillo, J. Martinez, O. Bassa, Virol J. 11 (2014) 149. doi:10.1186/1743-422X-11-149 [doi].

[75] F. Waggett, M.D. Shafiq, P. Bartlett, Colloids Interfaces. 1 (2018) 1.

[76] L. Qi, Z. Xu, X. Jiang, C. Hu, X. Zou, Carbohydrate Research. 339 (2004) 2693. doi:https://doi.org/10.1016/j.carres.2004.09.007.

[77] B. Canton, A. Labno, D. Endy, Nat Biotechnol. 26 (2008) 787. doi:10.1038/nbt1413.

[78] I.M. Helander, E.-. Nurmiaho-Lassila, R. Ahvenainen, J. Rhoades, S. Roller, International Journal of Food Microbiology. 71 (2001) 235. doi:https://doi.org/10.1016/S0168-1605(01)00609-2.

[79] M. Ferro, A. Doyle, Cell Biol Toxicol. 17 (2001) 205.

[80] A. Oslizlo, P. Stefanic, I. Dogsa, I. Mandic-Mulec, Proc Natl Acad Sci U S A. 111 (2014) 1586. doi:10.1073/pnas.1316283111 [doi].

[81] S.Y. Tan, S.L. Chua, Y. Chen, S.A. Rice, S. Kjelleberg, T.E. Nielsen, L. Yang, M. Givskov, Antimicrob Agents Chemother. 57 (2013) 5629. doi:10.1128/AAC.00955-13 [doi].

[82] C.G. Moreira, K. Palmer, M. Whiteley, M.P. Sircili, L.R. Trabulsi, A.F. Castro, V. Sperandio, J Bacteriol. 188 (2006) 3952. doi:188/11/3952 [pii].

[83] T.L. Moore, L. Rodriguez-Lorenzo, V. Hirsch, S. Balog, D. Urban, C. Jud, B. Rothen-Rutishauser, M. Lattuada, A. Petri-Fink, Chem Soc Rev. 44 (2015) 6287. doi:10.1039/c4cs00487f [doi].

[84] Y. Huang, Y. Cai, Y. Lapitsky, J Mater Chem B. 3 (2015) 5957.

[85] S. Lazzari, D. Moscatelli, F. Codari, M. Salmona, M. Morbidelli, L. Diomede, J Nanopart Res. 14 (2012) 920. doi:10.1007/s11051-012-0920-7 [doi].

[86] T. López-León, E.L.S. Carvalho, B. Seijo, J.L. Ortega-Vinuesa, D. Bastos-González, Journal of Colloid and Interface Science. 283 (2005) 344. doi:https://doi.org/10.1016/j.jcis.2004.08.186.

[87] M. Cetin, Y. Aktas, I. Vural, Y. Capan, L.A. Dogan, M. Duman, T. Dalkara, Drug Deliv. 14 (2007) 525. doi:785910386 [pii].

[88] A. Enriquez de Salamanca, Y. Diebold, M. Calonge, C. Garcia-Vazquez, S. Callejo, A. Vila, M.J. Alonso, Invest Ophthalmol Vis Sci. 47 (2006) 1416. doi:47/4/1416 [pii].

[89] J.-. OH, S.C. Chun, M. Chandrasekaran, J.-. OH, S.C. Chun, M. Chandrasekaran, Agronomy. 9 (2019) 21.

[90] P. Saha, A.K. Goyal, G. Rath, Trop J Pharm Res. 9 (2010) 483.

[91] A.R.M.A. El-Aziz, M.R. Al-Othman, M. Mahmoud, S. Shehata, N.S. Abdelazim, Curr Sci. 114 (2018) 2116.

[92] W. Fan, W. Yan, Z. Xu, H. Ni, Colloids and Surfaces B: Biointerfaces. 90 (2012) 21. doi:https://doi.org/10.1016/j.colsurfb.2011.09.042.

[93] Y. Huang, Y. Lapitsky, Journal of Colloid and Interface Science. 486 (2017) 27. doi:https://doi.org/10.1016/j.jcis.2016.09.050.

[94] M. Arteche-Pujana, L. Pérez-Álvarez, L.C. Cesteros-Iturbe, I. Katime, Carbohydrate Polymers. 94 (2013) 836. doi:https://doi.org/10.1016/j.carbpol.2013.01.082.

[95] G.V. Kumar, C. Su, P. Velusamy, Materials Letters. 180 (2016) 119. doi:https://doi.org/10.1016/j.matlet.2016.05.108.

[96] M.A. Razi, R. Wakabayashi, Y. Tahara, M. Goto, N. Kamiya, Colloids and Surfaces B: Biointerfaces. 164 (2018) 308. doi:https://doi.org/10.1016/j.colsurfb.2018.01.041.

[97] S.J. Jeon, M. Oh, W.S. Yeo, K.N. Galvao, K.C. Jeong, PLoS One. 9 (2014) e92723. doi:10.1371/journal.pone.0092723 [doi].